American Journal of Physical Chemistry
2021; 10(4): 67-80
http://www.sciencepublishinggroup.com/j/ajpc
doi: 10.11648/j.ajpc.20211004.14
ISSN: 2327-2430 (Print); ISSN: 2327-2449 (Online)

Thermochemistry and Reaction Kinetics of Secondary Ethyl Radical of Methyl Ethyl Sulfide, $CH_3SCH•CH_3$, with $^3O_2$ to $CH_2SCH(OO•)CH_3$

Guanghui Song, Joseph Bozzelli*, Hebah Abdel-Wahab*

Department of Chemical, Biological and Pharmaceutical Engineering, New Jersey Institute of Technology, University Heights, Newark, USA

Email address:
bozzelli@njit.edu (J. Bozzelli), dr.heathera@gmail.com (H. Abdel-Wahab)

*Corresponding author

To cite this article:
Guanghui Song, Joseph Bozzelli, Hebah Abdel-Wahab. Thermochemistry and Reaction Kinetics of Secondary Ethyl Radical of Methyl Ethyl Sulfide, $CH_3SCH•CH_3$, with $^3O_2$ to $CH_2SCH(OO•)CH_3$. *American Journal of Physical Chemistry.* Vol. 10, No. 4, 2021, pp. 67-80.
doi: 10.11648/j.ajpc.20211004.14

Received: October 4, 2021; **Accepted**: October 29, 2021; **Published**: November 12, 2021

Abstract: The quantum Rice-Ramsperger-Kassel (QRRK) theory is used to analyze the reaction between the activated $CH_3SCH•CH_3$ and molecular oxygen to account for further reaction and collisional and deactivation. hydroxyl radicals initiate the oxidation of Methyl ethyl sulfide ($CH_3SCH_2CH_3$) and MES (methylthioethane) under combustion conditions. The CBS-QB3 and G3MP2B3 composite and M062X/6-311+G(2d, p) DFT methods was used to study the thermochemical properties of reactants, products and transition states. These thermochemical properties are used for the calculations for kinetic and thermochemical parameters. Under high pressure and low temperature, isomerization and stabilization of the $CH_3SCH(OO•)CH_3$ adduct is of importance. Under atmospheric pressure and at temperatures between above 600 ~ 800 K reactions of the chemically activated peroxy adduct become important relative to stabilization. The reaction between $CH_3SCH•CH_3$ and O_2 forms an energized peroxy adduct $CH_3SCH(OO•)CH_3$ with a calculated well depth of 30.2 kcal/mol at the CBS-QB3 level of theory. Kinetic parameters are calculated using the thermochemical properties of products, reactants and transition states obtained using under CBS-QB3 method of calculation. At temperature below 500 K, Stabilization of $CH_3SCH(OO•)CH_3$ adduct is of importance. Temperature of 500-900 K, is optimal for intramolecular hydrogen shift and the isomerization of $CH_3SCH(OO•)CH_3$ adduct. At temperature above 800 K, all of the subsequent reaction paths are of importance. For a reaction to move forward under pressure 1-4 atm, the recommended optimal temperature is between 600-800 K. A new pathway for the $CH_3SCH(OO•)CH_3$ adduct is observed, the attachment of peroxyl oxygen radical to sulfur followed by carbon-sulfur bond dissociation and formation of oxygen-sulfur and oxygen-carbon double bonds.

Keywords: Methyl Ethyl Sulfide, Thermochemistry, Kinetics, Oxidation

1. Introduction

Biofuels contain lots of sulfur containing substances. [1] In combustion science, the kinetics for the decomposition of sulfur compounds under different pressure and temperature play an important role. [2] The reaction between O_2 and $CH_3S(OH)CH_3$ was studied by Gross et al using DFT methods and *ab initio* theory. [5] Information on the partial oxidation for sulfur hydrocarbons with three or more carbons and the kinetics of combustion is still in need. [6, 7]

The reaction mechanisms and kinetics for the destruction of different types of sulfur compounds under varied temperature and pressure play an important role in combustion science. [2] A better understanding of the combustion and partial oxidation of sulfur compounds is important for the reduction and prevention of sulfuric oxides that causes destruction to the environment, buildings and human health. [3] Gargurevich investigated the combustion mechanisms and kinetics of H_2S under Claus Furnace conditions based on the reviews of recently published reaction mechanisms and kinetics modeling. [4] Gross et al theoretically studied the reaction between $CH_3S(OH)CH_3$ and O_2 using *ab initio* theory and DFT methods. [5] There is, however, still a need for information on the kinetics of

combustion and for the partial oxidation for sulfur hydrocarbons with three or more carbons in the atmosphere. [6, 7] Significant amount of methyl ethyl sulfide (MES) and $CH_3SCH_2CH_3$, methylthioethane are emitted into the atmosphere due to biological activities in the sea. [8] MES has a negative effect on environment and atmosphere by its generation and contribution in the production of smog and sulfuric oxides. [9] The oxidation of MES under combustion conditions and higher temperature is of value for kinetic modeling.

Kinetics and Thermochemistry of $C_2H_5 + O_2$ and the chemically activated and stabilized $CH_3CH_2OO•$ adduct was studied by Sheng and Bozzelli. [19] Thermodynamic and kinetic analysis on the reaction of $CH_3SCH_2• + O_2$ was reported by Jin and Bozzelli. [20] In 2014, Thermochemistry, kinetics and reaction paths on the tert-isooctane radical reaction with O_2 was studied by Snitsiriwat and Bozzelli [21].

Structural and thermochemical properties of the stable molecules of the sulfur peroxides and alcohols of MES and all of its partial oxidation intermediates was previously studied by the Song et. al. [22, 23]

This study includes intramolecular isomerization (hydrogen transfers), beta scissions and intramolecular addition reaction of the peroxy oxygen radical to the sulfur atom, resulting peroxy oxygen–oxygen and the methyl carbon-sulfur bond cleavages and in oxygen–sulfur and oxygen–carbon π bond formation on the sulfur atom in the carbon components.

2. Calculation Methods

Thermochemical properties of the parent molecules and their radical fragments were calculated using several density functional theory and composite *ab initio* computation chemistry methods in the Gaussian 09 program suite. [18-20] The different levels of calculation used in this study include the M06-2x/6-311+g(2d,p) density functional theory (DFT) method and the *ab initio* CBS-QB3 and G3MP2B3 composite methods. The composite CBS-QB3 calculation method has been used for the thermochemical properties, in order to achieve improvements on the accuracy over the DFT methods. The CBS-QB3 method utilizes the B3LYP/6-311G(2d,d,p) level of theory to get the optimized lowest energy geometries and to calculate frequencies, it then uses CCSD(T), MP4 (SDQ) and MP2 calculations to determine single point energies. [21, 22] The G3MP2B3 method is a modified version of G3MP2 method that uses the geometries and vibrational energies obtained from B3LYP/6-31G(d) calculations. [23-25] The energy of each transition state was calculated based on the energy of corresponding reactant plus the calculated energy difference between the transition state and the reactant.

Molecular structures and vibrational frequencies were determined at the B3LYP/6-311G (2d,d,p) in the CBS-QB3 level of calculation, which is considered accurate for the calculation of electronic structure and energies of the first and second row atoms. [26-28] The Complete Basis Set-QB3 multi-level method was developed by the research group of G. Peterson [26, 27] and Kiselev *et al*. [28] The CBS-QB3 multilevel method is based on the optimized geometries at the B3LYP/6-311G(2d,d,p) level.

The entropy and heat capacity of molecules, radicals and transition states as a function of temperature were from the optimized structures, moments of inertia, vibration frequencies, symmetries, electronic multiplicity, and molecular mass. All of the optimized lowest energy structures of reactants and products were identified as having no imaginary frequency. Transition states were identified with one imaginary frequency related to the vibration that demonstrates the transitional motion between the reactant and the product. Contributions of translation, external rotation and vibrations were determined with standard formulas from statistical mechanics. Contributions to the entropy and heat capacity of each molecule and radical from translation, vibrations and external rotation were determined using the Statistical Mechanics for Heat Capacity and Entropy, C_p and S (SMCPS) program. The SMCPS program utilizes the rigid-harmonic oscillator approximation from the optimized structures obtained at the B3LYP/6-311G(2d,d,p) level. [29, 30] The number of optical isomers, when they exist, and the spin degeneracy of unpaired electrons were also incorporated into the calculation of S°_{298K}. The SMCPS program utilizes the rigid-harmonic oscillator approximation from the optimized structures obtained in the CBS-QB3 calculation. [31, 32] The scaling factor for zero-point vibrational energy is 0.99. [31-34]

The internal rotor potential energy diagrams and the lowest energy optimized conformer for each target, parent peroxide molecule and radical were determined using the B3LYP/6-31+G(d,p) level DFT calculations. Internal rotor analysis was performed on each C—S, C—C, C—O or O—O single bond rotor to determine the lowest energy structures. All rotors were re-scanned once a lower energy conformer was found compared to the initial energy conformer, until the lowest energy geometry was identified.

Contributions from all of the hindered internal rotors to S°_{298} and $C_p(T)$ were determined using the Rotator program. [35] The Rotator program calculates the thermodynamic functions from hindered rotations with arbitrary potentials based on the method developed by Krasnoperov, Lay and Shokhirev. [36] This technique employs expansion of the hindrance potential in the Fourier series, calculation of the Hamiltonian matrix in the basis of the wave functions of free internal rotors, and subsequent calculation of energy levels by direct diagonalization of the Hamiltonian matrix. [37] Internal rotor torsion frequencies were omitted from the SMCPS frequency sets and internal rotor contributions were added separately. The contributions from the identified torsion frequencies were omitted and replaced with the hindered rotor contributions. The moments of inertia for each of the two components of the rotor were calculated. [38-40] Summation of the SMCPS and Rotator contributions gives the total entropy and heat capacity for each species.

The kinetics of O_2 addition to the radical sites of methyl ethyl sulfide and their reverse reactions were determined based on the Variational Transition State Theory (VTST). The M06-2x/6-311+g(2d,p) level C—OO• bond length scans were performed with calculation of optimized structure, energy and vibration frequencies at each 0.05 Å step. A complete set of thermochemical properties are calculated for the different transition state structures at each step. Rate constants are subsequently calculated from the reactant to each structure at temperatures of 300 to 2000 K. The minimum rate constant is taken across the temperature – bond length data set, for each temperature. The minimum set of rate constants over the temperature range is fit to the modified Arrhenius rate constant form. [41]

High-pressure limit reaction rate constants (k_∞, s^{-1} or cm^3 mol^{-1} s^{-1}) were determined based on the canonical transition state theory. The values of k_∞ were fit to the three-parameter form of the Arrhenius equation to yield the parameters of A, n, and E_a over the temperature range of 200-3000K:

$$k_\infty = \Gamma(T)*A*(T\text{^}n) *\exp(-E_a/RT)$$

Where activation energies of reactions (E_a) are calculated as $E_a = [\Delta H_f^o{}_{298}$ (TS) $-\Delta H_f^o{}_{298}$ (Reactant)].

The quantum mechanical tunneling correction (Γ, dimensionless) was calculated using Eckart's method; [42-44]

The entropy differences between the reactants and the transition states ($\Delta S^{\neq}$) over the temperature range of 200-3000 K were used to determine the pre-exponential factor (A, s^{-1} or cm^3 mol^{-1} s^{-1}). The values of A are expressed by:

$$A\ (T) = (\kappa_b T/h_p) \exp(\Delta S^{\neq}/R)$$

Where h_p is the Planck's constant and κ_b is Boltzmann's constant, R is gas constant and R = 1.987cal $mol^{-1}K^{-1}$. [29, 34, 45, 46]

The high pressure limit parameters are calculated based on the thermochemical properties of reactant, product and transition state geometries optimized under the CBS-QB3 level. Temperature and pressure-dependent rate constants are calculated using the multichannel, multifrequency Quantum Rice-Ramsperger-Kassel (QRRK) analysis for $k(E)$ based on a master equation analysis for falloff and stabilization as implemented in the CHEMASTER code. [29, 47] Reduced sets of three vibrational frequencies and their degeneracy plus energy levels of one external rotor are used to yield the ratio of density of states to partition the coefficient, $\rho(E)/Q$ for each adduct (isomer in the chemical activation or dissociation reaction system). The Master Equation analysis used an exponential-down model for the energy transfer function with ($\Delta E_{down}{}^o$) 900 cal mol^{-1} for N_2 as the third body. [48] Rate constants, k(E), were evaluated by using incremental energy bins of 1.0 kcal mol^{-1} up to 75 kcal mol^{-1} above the highest barrier. Lennard-Jones parameters, σ (Å), and ε/k (K) were obtained from tabulations and from an estimation method based on molar volumes and compressibility. [49] High-pressure-limit elementary-rate parameters were used as input data to the QRRK calculations.

3. Results and Analysis

3.1. Reaction Pathways and Geometries of Optimized Transition States

According to the recent studies by Mansilla *et al*. [17] and Cao *et al*. [8], the partial oxidation of MES in th from each MES molecule by one hydroxyl radical: [10-13, 17, 50, 51]

$$CH_3SCH_2CH_3 + HO• \rightarrow CH_2•SCH_2CH_3 + H_2O$$

$$CH_3SCH_2CH_3 + HO• \rightarrow CH_3SCH•CH_3 + H_2O$$

$$CH_3SCH_2CH_3 + HO• \rightarrow CH_3SCH_2CH_2• + H_2O$$

The radicals formed after loss of one hydrogen atom from different carbon sites will subsequently react with O_2 to form active sulfuric alkyl peroxy radicals: [8, 14, 16, 50]

$$CH_2•SCH_2CH_3 + O_2 \rightarrow CH_2(OO•)SCH_2CH_3$$

$$CH_3SCH•CH_3 + O_2 \rightarrow CH_3SCH(OO•)CH_3$$

$$CH_3SCH_2CH_2• + O_2 \rightarrow CH_3SCH_2CH_2OO•$$

This paper focuses on the thermochemistry, reaction paths and kinetics of the $CH_3SCH•CH_3$ radical reaction with O_2 and subsequent reactions.

The elementary reaction steps investigated in this paper belong to the following categories: [8, 29, 46, 47, 50, 52]

Forward association and reverse dissociation reactions of the $CH_3SCH•CH_3$ radical with O_2 are investigated by VTST;

Intramolecular hydrogen transfer from carbon the three carbon sites to the peroxy oxygen radical (TS211, TS231); plus the H-transfer from the ipso carbon to the peroxy oxygen, which further reacts with no barrier to form an aldehyde plus hydroxyl radical (TS221);

Molecular dissociation caused by C—S bond cleavage (TS213, TS234);

Reactions to cyclic ether ring formation plus OH radical (TS212, TS232);

Intramolecular addition of peroxy oxygen radical to the sulfur atom with simultaneous cleavage of the weak O—O and C—S bonds, resulting information of two products with C=O and S=O double bonds (TS251);

HO_2 elimination to generate CSC=C (TS233, TS241)

The optimized lowest energy structures and thermochemical properties of MES along with its radicals and the peroxide molecules and radicals have already been previously studied [7].

Transition states are characterized as having only one negative eigenvalue of Hessian (force constant) matrices. The absence of imaginary frequency verifies that the structures are true minima at the respective levels of theory. The optimized lowest energy transition state conformers from the CBS-QB3 level are drawn in Figure 2.

$CH_3SCH(OO•)CH_3$ ←TS211→ $H_2C•SCH(OOH)CH3$ --TS212→ H_2 CSC-C H_3+ OH
--TS213→ CH_2S + OH + $CH_3CH=O$

$CH_3SCH(OO•)CH_3$ --TS221→ $CH_3SC•(OOH)CH_3$ → $CH_3SC(=O)CH_3$ + OH

$CH_3SCH(OO•)CH_3$ ←TS231→ $CH_3SCH(OOH)CH_2•$ --TS232→ H_2 CSC-C H_2+ OH
--TS233→ $CH_3SCH=CH_2$+ HO2
--TS234→ CHS• + CH_2=COOH

$CH_3SCH(OO•)CH_3$ --TS241→ $CH_3SCH=CH_2$ + HO_2

$CH_3SCH(OO•)CH_3$ --TS251→ $CH_3CH=O$ + CHS˙=O

$CH_3SCH(OO•)CH_3$ ←VTST→ $CH_3SCH•CH_3$ + O_2

Figure 1. *Subsequent reaction steps of $CH_2SCH(OO•)CH_3$ radical along with the numbering of the corresponding transition states.*

TS211

CSC(OO•)C → C•SC(OOH)C

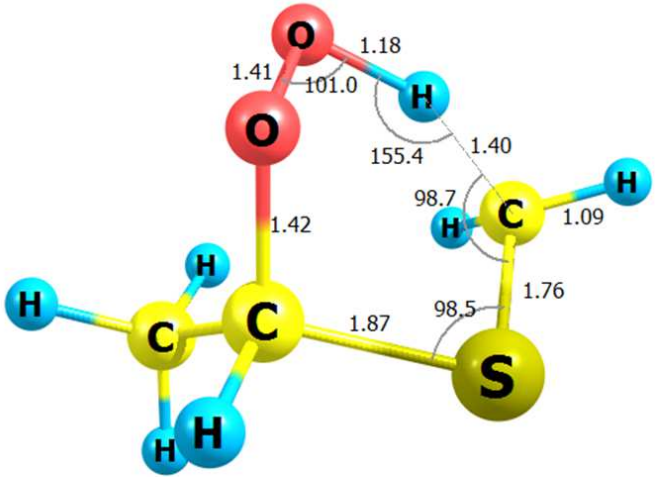

TS212

C•SC(OOH)C → CSC-C + OH

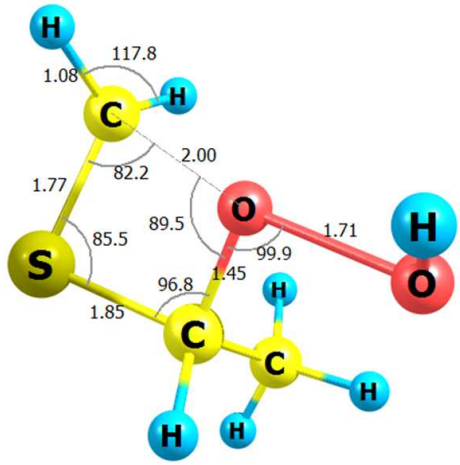

TS213

C•SC(OOH)C → CH_2=S + CC=O + OH

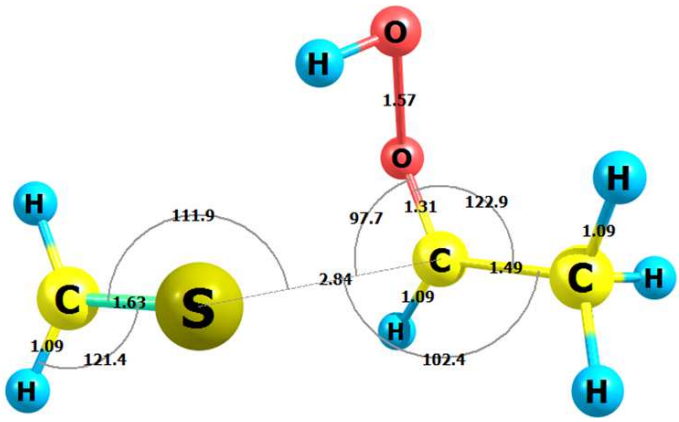

TS221

CSC(OO•)C → CSC(=O)C + OH

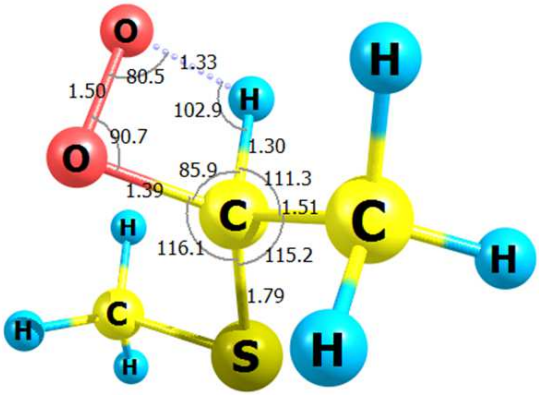

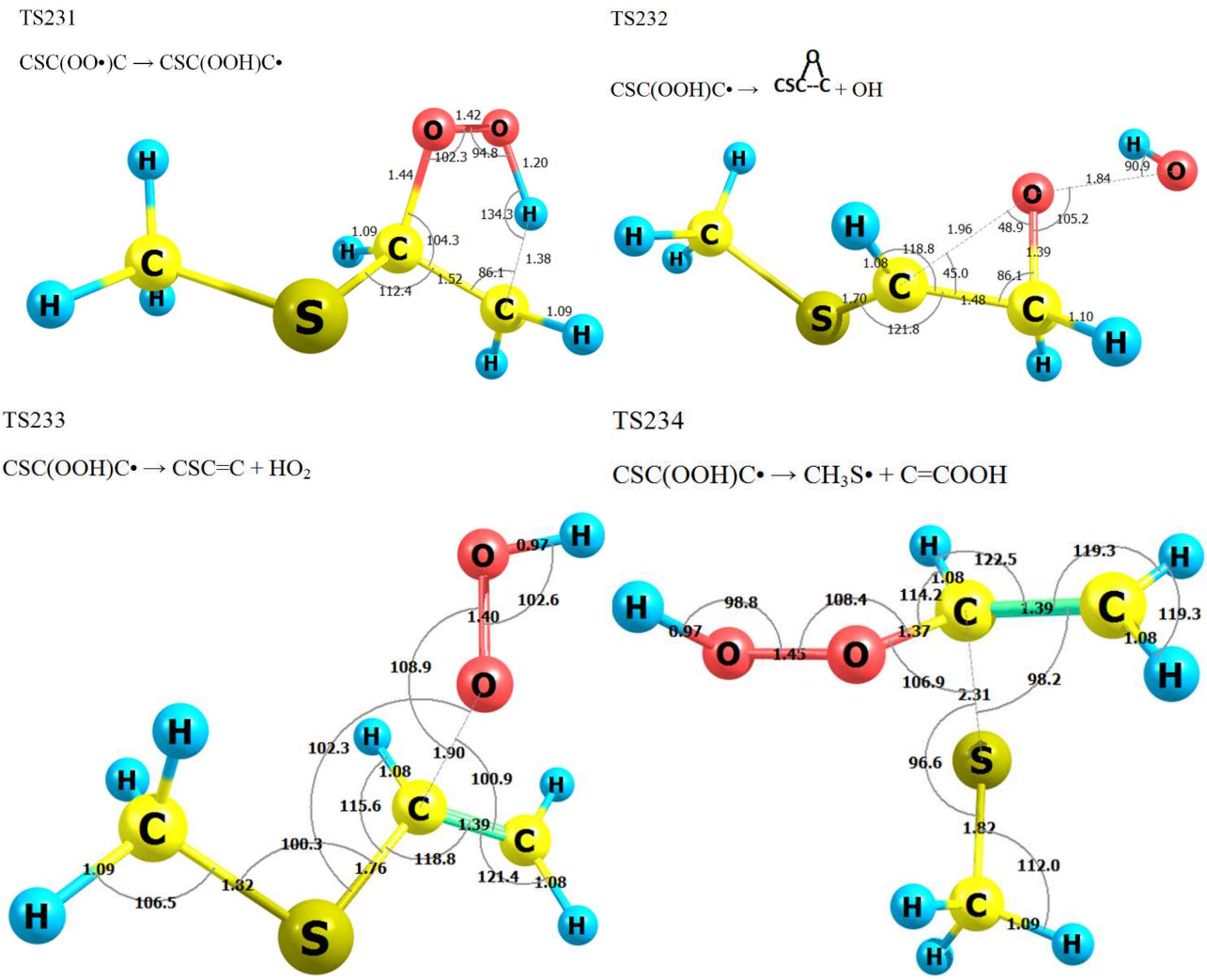

Figure 2. *Geometry of lowest energy conformer of transition states at 298K calculated under CBS-QB3 level.*

3.2. Variational Transition State Theory (VTST) Analysis

A Zero-point corrected potential energy surface for the RC—OO• bond is illustrated in Figure 3. Potential energy scans were performed along the R—OO• → R• + O_2 dissociation path in the MES peroxide bond cleavage reaction at 0.05 Å intervals. Frequency and thermodynamic calculations were performed at each of the points along the potential energy surface. Thermochemical properties and rate constants as a function of temperature were calculated at each point along the potential energy surface.

Variational transition kinetics were calculated based on thermochemical data obtained at the M062X/6-311+G(2d,p) level. Each point on the M062X reaction potential energy scan, was scaled by a factor that accounted for the ratio of the CBS-QB3 reaction enthalpy to the M062X reaction energy in order to improve the precision of dissociation energy points. Rate constants were calculated as a function of temperature at each bond distance. The overall minimum rate constant at each temperature was then determined. Rate constants (T) were fit to the three-parameter form of the Arrhenius equation to yield the rate parameters A, n and E_a listed in Table 1.

The VTST plot of O_2 separation from peroxide radical indicates the BDE of •OO—$CH_2SCH_2CH_3$ is about 30.0 kcal/mol, close to the value of 30.2 kcal/mol that is indicated by the PE diagram in Figure 4. For comparison to hydrocarbons, Sheng et. al. reported values for CH_3CH_2—OO• BDE of 35.32 kcal/mol by CBS-QB3 and 35.5 kcal/mol by and B3LYP/6-31G(d, p) level VTST analysis. Snitsiriwat's et. Al reported R—COO• BDE values in tertiary carbon of -isooctane hydroperoxide based on CBS-QB3 calculation and B3LYP/6-31G(d, p) level VTST scans at 34.7 kcal/mol and 33.5 kcal/mol, respectively. [48] Similar to the dissociations of Jin, Sheng and Snitsiriwat's C—OO• bonds, dissociation of the $CH_2SCH(—OO•)CH_3$ bond undergoes with no barrier other than ΔHrxn. [29, 46, 47] For Snitsiriwat's tert-isooctane hydroperoxide C—OO• bond dissociation, the TS was 3.0 Å at T=300 K. [47]

The normalized energy versus bond length plot in Figure 3 indicates that transition state occurs between the •OO—$CH_2SCH_2CH_3$ bond length of 2.0 ~ 2.3 Å. Based on the analysis to the rate constants of both the association and dissociation reactions, and the M062X method was able to converge on an optimized TS geometry with the C—OO• bond length of 2.15 Å for $CH_2SCH(--OO•)CH_3$. It appears

that compared to saturated hydrocarbons, with only carbon and hydrogen, the presence of sulfur reduces the chemical activation energy and the transition state C—OO• bond length for O_2 association to carbon atoms adjacent to the sulfur moiety by about 7 kcal/mol and 0.8 Å, respectively.

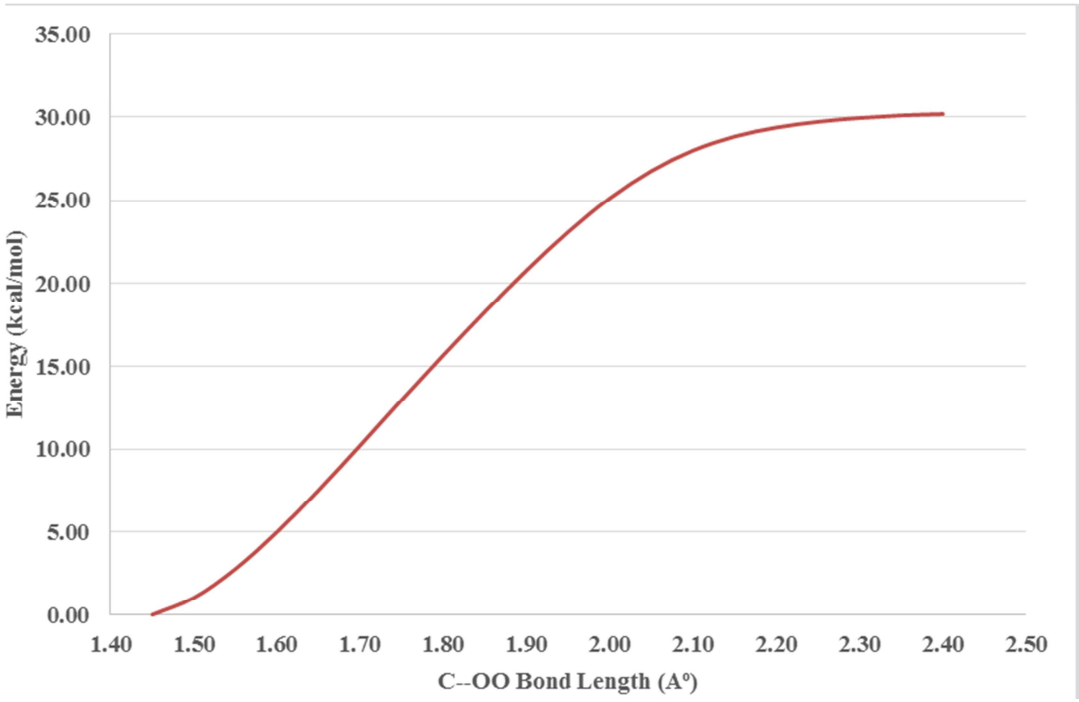

Figure 3. *The $CH_2SCH(—OO•)CH_3$ bond length scan for VTST calculation.*

Table 1. *Elementary rate parameters from VTST analysis for $CH_2SCH(OO•)CH_3$.*

Association			Dissociation		
A^a	n	E_a (kcal)	A^b	n	E_a (kcal)
2.86E+3	2.24	-1.61	8.80E+12	0.33	29.41

[a]The unit of pre-exponential factor for the association reaction is $cm^3\ mol^{-1}\ s^{-1}$.
[b]The unit of pre-exponential factor for the dissociation reaction is s^{-1}.

3.3. Thermochemical and Kinetic Analysis

The energy barriers (E_a) and reaction enthalpy (ΔH_{rxn}) for the reactions of $CH_2SCH(OO•)CH_3$ under the M06-2X/6-311+G(2d,p), G3MP2B3 and CBS-QB3 calculation levels are listed in Table 2. The energy of each transition state structure is calculated from the corresponding reactant plus the energy difference between the transition state and the reactant. The CBS-QB3 calculation shows good agreement with the M062X/6-311+G(2d,p) calculation in the intramolecular hydrogen shift and β-scission reactions. There is however a 4 ~ 7 kcal/mol difference in the E_a and ΔH_{rxn} values of the reactions involving ring formation and for O• attachment to S. The two composite methods CBS-QB3 and G3MP2B3 agree reasonably well for ΔH for each of the reactions and TST's.

Table 2. *E_a and ΔH_{rxn} values under different calculation levels (kcal/mol).*

Reactions	CBS-QB3		M062x/6-311+G(2d,p)		G3MP2B3	
	E_a	ΔH_{rxn}	E_a	ΔH_{rxn}	E_a	ΔH_{rxn}
CSC(OO•)C → C•SC(OOH)C	18.3	8.3	20.7	12.1	20.4	10.3
C•SC(OOH)C →  + OH	26.0	-14.3	30.9	-16.1	27.1	-16.1
C•SC(OOH)C → CH_2=S + CC=O + OH	22.1	-8.7	22.5	-7.6	24.9	-12.1
CSC(OO•)C → CSC(=O)C + OH	36.3	-36.3	39.5	-35.3	38.7	-38.3
CSC(OO•)C → CSC(OOH)C•	34.6	16.6	37.7	17.0	-----	16.6
CSC(OOH)C• →  + OH	7.8	-14.9	14.4	-15.8	10.9	-16.2
CSC(OOH)C• → CSC=C + HO_2	15.3	6.2	18.0	6.3	16.3	4.3
CSC(OOH)C• → CH_3S• + C=COOH	9.0	8.5	9.8	8.8	10.6	7.2
CSC(OO•)C → CSC=C + HO_2	28.5	22.8	30.1	23.3	27.7	20.9
CSC(OO•)C → CC=O + CS•=O	31.1	-53.3	38.9	-46.8	32.2	-53.3

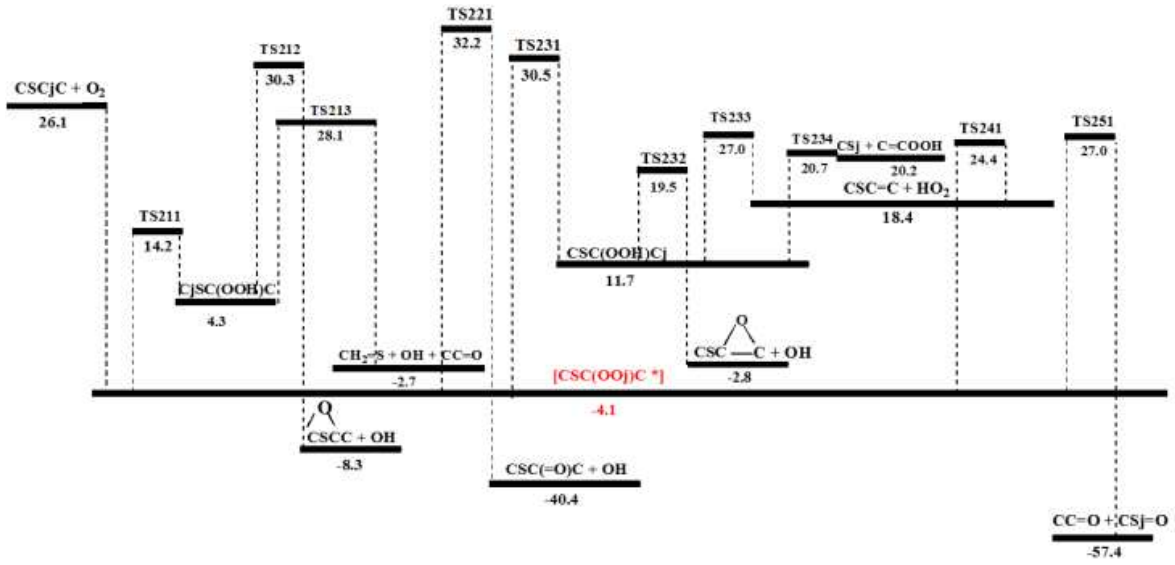

Figure 4. *CBS-QB3 level potential energy diagram for $CH_3SCH•CH_3$ + O_2 reaction system.*

The potential energy diagram in Figure 4 are based on the CBS-QB3 level potential energy calculations for each species. The enthalpies of formation for the peroxides, radicals, aldehydes and ketones of MES are from our previous work,[53, 54] while those of O_2, OH, HO_2 are from Ruscic *et al*. [56] The total enthalpies of products for each reaction step in Figure 4 are calculated based on the difference between the CBS-QB3 total energies of the reactants and the products.

TS211 in Figure 4 illustrates the intramolecular transfer of H atom from the methyl carbon of CSC(OO•)C to the peroxy radical site, through a six member ring TST structure. The reaction results in formation of C•SC(OOH)C, and has a barrier of 18.3 kcal mol^{-1}.

The methyl radical on this newly formed C•SC(OOH)C intermediate can undergo a substitution reaction into the carbon bonded oxygen of the hydroperoxide to form a cyclic four-member ring 'thiol–ether' with elimination of an OH radical. The reaction barrier is 26.0 kcal mol^{-1}.

The C•SC(OOH)C radical can also undergo C•S--C(OOH)C bond beta scission to form CH_2=S and CC•OOH over a barrier of 23.8 kcal/mol. The CC•OOH radical is unstable and instantaneously undergoes β-scission forming a CC=O π bond and CC=O—OH scission to the lower energy products CC=O and OH.

TS221 represents the formation of the CSC(=O)C ketone plus hydroxyl radical via intramolecular transfer of the H atom from the secondary carbon, i.e. the carbon of the peroxide group to the peroxy radical site, forming an unstable the [CSC•(OOH)C]*. The CSC•(OOH)C is unstable and instantaneously forms a new CSC=O π bond of about 80 kcal mol-1; while cleaving the weak (~ 45 kcal mol-1 [CSC=O—OH] bond forming CSC(=O) ketone and OH radical. This ketone formation path has a barrier for the peroxy oxygen attack on the ipso hydrogen of 36.3 kcal/mol.

TS231 involves the intramolecular transfer of a H atom from the primary carbon on the ethyl group of CSC(OO•)C to the peroxy radical site, through a five member ring TST structure, resulting in formation of CSC(OOH)C•.

The TS231 has a 34.6 kcal mol^{-1} barrier. The higher barrier is a result of strain in the *5-member ring* and the stronger C—H bond of this primary carbon site on the ethyl group.

Following this intramolecular hydrogen transfer, the newly formed methyl radical [CSC(OOH)C•] can undergo substitution into the peroxide oxygen, TS232. This has a low barrier of 7.8 kcal/mol for formation of a 4-member epoxy ring, CSy(COC) plus OH radical.

β-scission of the CS--C(OOH)C• bond generates CH_3S• and C=COOH, with a barrier of 9.0 kcal/mol that is represented by TS234.

The CSC(OOH)C• radical can also undergo HO_2 elimination to generate CSC=C, with a barrier of 15.3 kcal/mol shown as TS233.

TS241 represents HO_2 molecular elimination from the CSC(OO•)C adduct, generating CSC=C with a barrier of 28.5 kcal/mol. These products are the same as those of the path represented by TS233.

The dissociation of CSC(OO•)C into CC=O and CS•=O is illustrated by TS251 and occurs over a barrier of 31.1 kcal mol^{-1}. The peroxy oxygen radical adds to the sulfur. Bond formation between peroxy oxygen and sulfur initiates, along with cleavage of both the sulfur—ethyl carbon and the CH_3CH_2O—OS•CH_3 peroxide bond. Two π bonds are formed: CH_3S•=O and CH_3CH_2=O, and the sulfur–ethyl carbon bond is cleaved.

The intramolecular hydrogen transfer from the primary ethyl carbon to the carbon peroxyl radical (5-member ring) has a 16.3 kcal/mol higher barrier and is 8.2 kcal/mol more endothermic than the 6- member ring TST for the hydrogen transfer from the methyl carbon on the sulfur to the peroxyl radical site.

Following hydrogen shift, a barrier of 26.0 kcal/mol is required for the y(CSCO)C ring structure formation by C•SC(OOH)C that has a ΔH_{rxn} value of -12.6 kcal/mol.

The barrier required for the CSy(COC) ring formation from CSC(OOH)C• is 7.8 kcal/mol with the ΔH_{rxn} value of -14.9 kcal/mol.

The CSC(=O)C ketone formation has a barrier of 36.3 kcal/mol, which is the highest among all the subsequent reactions of CSC(OO•)C.

The dissociation into CC=O plus CS•=O and the CSC(=O)C ketone formation paths are the more exothermic reactions for CSC(OO•)C, with ΔH_{rxn} value of -53.3 and -36.3 kcal/mol, respectively. Both are more exothermic than reactions leading to a ring structure.

There are two routes from the initial peroxy radical CSC(OO•)C to CSC=C + HO_2: The direct HO_2 via TS241 has a 6.1 kcal/mol lower barrier than the TS231path via the ethyl primary radical hydroperoxide CSC(OOH)C•.

The chain branching unimolecular dissociation reaction of CSC(OO•)C → CSC(O•)C + O• has a reaction energy of 59.6 kcal/mol. This is some 23 kcal mol^{-1} higher than the highest barriers in the unimolecular reactions presented. The rate constant of this channel is not important at the temperatures and pressures of this study.

The ideal gas-phase thermochemical properties of species calculated from the CBS-QB3 level for the lowest energy geometries are listed in Table 3.

Table 3. *Ideal gas-phase thermochemical properties.*

Species	$\Delta H_f°_{298}$ [a]	$S°_{298}$ [b]	C_{p300} [b]	C_{p400}	C_{p500}	C_{p600}	C_{p800}	C_{p1000}	C_{p1500}
CSC•C[c]	26.10	66.09	16.86	21.36	25.49	29.04	34.70	39.00	45.83
C•SC(OOH)C[c]	4.30	74.75	21.86	27.41	32.13	36.01	41.93	46.30	53.25
CSC(OO•)C[c]	-4.10	72.18	20.98	26.75	31.86	36.16	42.78	47.63	55.11
CSC(OOH)C•[c]	11.70	75.14	22.02	27.65	32.39	36.26	42.13	46.45	53.33
$CH_3SC(=O)CH_3$[c]	-49.72	69.91	20.03	24.71	28.87	32.41	37.96	42.09	48.54
CH_2=S [35]	27.60	55.13	9.05	10.29	11.46	12.45	14.02	15.21	17.11
y(CSCO)C	-17.20	69.16	18.92	24.39	29.23	33.27	39.41	43.82	50.50
CSy(CCO)	-11.70	69.23	18.36	23.66	28.31	32.14	37.96	42.16	48.61
$CH_3SCH=CH_2$	15.50	66.16	16.52	20.95	24.83	28.08	33.15	36.94	42.96
CH_3S•	29.40	57.69	10.80	12.54	14.07	15.38	17.51	19.16	21.86
CH_3S•=O	-17.80	62.48	12.16	14.43	16.42	18.07	20.64	22.54	25.53
O_2 [57]	0.00	48.90	7.02	7.20	7.43	7.60	8.00	8.20	8.60
OH [57]	8.89	43.88	7.17	7.08	7.06	7.06	7.15	7.33	7.87
$CH_3CH=O$ [57]	-39.60	63.00	13.00	15.50	18.00	20.20	23.80	26.60	30.90
HO_2 [57]	2.90	54.60	8.30	8.80	9.40	9.90	10.70	11.30	12.30
CH_2=CHOOH [57]	-9.20	73.00	18.40	21.60	24.40	26.70	30.10	32.50	36.20
TS211	14.23	76.32	24.85	31.48	37.04	41.54	48.23	52.94	59.98
TS212	30.34	84.46	29.43	35.40	40.30	44.23	50.13	54.45	61.31
TS213	28.13	90.33	29.07	34.27	38.78	42.51	48.29	52.60	59.46
TS221	32.20	84.38	28.40	34.31	39.42	43.65	50.12	54.78	61.85
TS231	30.49	76.95	23.79	30.19	35.60	39.98	46.51	51.13	58.08
TS232	19.53	91.21	29.87	35.37	40.11	44.00	49.96	54.34	61.28
TS233	26.98	78.05	24.27	29.84	34.52	38.33	44.14	48.42	55.29
TS234	20.68	78.57	24.03	29.55	34.24	38.08	43.95	48.28	55.20
TS241	24.44	78.23	24.36	30.39	35.58	39.87	46.34	50.96	57.95
TS251	27.03	78.98	26.33	32.01	36.94	41.05	47.41	52.08	59.34

[a] Units in kcal mol^{-1}. [b] Units in cal mol^{-1} K^{-1}. [c] Previous work by the same author.

The elementary high-pressure limit Arrhenius rate parameters for the forward and reverse reactions are given in Table 4.

The kinetic rate constants representing •OOCSCC isomerization by intramolecular H transfer reactions have quantum tunneling corrections added to the *ab initio* rate coefficients. The tunneling corrections for the intramolecular hydrogen atom transfer reactions are listed in Table 5.

Table 4. *Elementary High Pressure Rate Parameters by CTST.*

Reaction	$k = A(T)^n \exp(-\frac{E_a}{RT})$ (300≤ T/K≤ 2000)		
	A(s^{-1})	n	E_a (kcal mol^{-1})
CSC(OO•)C → C•SC(OOH)C	3.8E+7	0.9	1.8E+4
C•SC(OOH)C → CSC(OO•)C	8.5E+8	0.1	9.7E+3
C•SC(OOH)C →  + OH	1.5E+9	0.4	2.6E+4
C•SC(OOH)C → CH_2=S + CC=O + OH	4.5E+12	0.1	2.4E+4
CSC(OO•)C → CSC(=O)C + OH	8.0E+7	1.1	3.6E+4
CSC(OO•)C → CSC(OOH)C•	1.7E+9	0.9	3.4E+4
CSC(OOH)C• → CSC(OO•)C	3.4E+8	0.6	1.8E+4
CSC(OOH)C• →  + OH	6.2E+8	0.8	7.6E+3
CSC(OOH)C• → CSC=C + HO_2	1.6E+11	0.4	1.6E+4
CSC(OOH)C• → CS• + C=COOH	5.3E+9	1.2	8.7E+3
CSC(OO•)C → CSC=C + HO_2	1.5E+9	1.1	2.8E+4
CSC(OO•)C → CC=O + CS•=O	1.3E+10	0.3	3.1E+4

Table 5. *Quantum tunneling corrections for CSC(OO•)C isomerization by intramolecular H transfer and their reverse reactions.*

Temperature (K)	Reactions			
	CSC(OO•)C → C•SC(OOH)C	C•SC(OOH)C → CSC(OO•)C	CSC(OO•)C → CSC(OOH)C•	CSC(OOH)C• → CSC(OO•)C
298	46	26	1150	616
300	46	26	1150	616
350	15.1	10.4	500	300
400	6.1	5.4	46	37
500	3.2	3.1	6.1	6.1
600	2.1	2.1	3.2	3.2
700	1.5	1.5	2.1	2.1
800	1.5	1.5	2.1	2.1
900	1.5	1.5	1.5	1.5
1000	1.2	1.2	1.5	1.5
1100	1.2	1.2	1.5	1.5
1200	1.2	1.2	1.5	1.5
1400	1.2	1.2	1.2	1.2
1500	1.2	1.2	1.2	1.2
1600	1.1	1.1	1.2	1.2
1800	1.1	1.1	1.2	1.2
2000	1.1	1.1	1.2	1.2

Figures 5 and 6 gives the plots of reaction rate constants versus 1000/T(K) from 298-2000 K under the pressures of 1 and 4 atm, respectively. 4 atm is chosen as the typical pressure in the diesel engine.

The temperature has significant effect on the rates of each reaction path under both pressures. Meanwhile, increasing the pressure from 1 to 4 atm does not significantly change the rate of any elementary reaction step under each temperature. Stabilization of and HO_2 elimination from $CH_3SCH(OO•)CH_3$ are both important at room temperature under two pressures. A low temperature enhances CSC•C activation by O_2. The two paths of $CH_3SCH(OO•)CH_3$ isomerization by intramolecular hydrogen shift both become more important at temperatures between 400-1000 K. The rates of molecular dissociations caused by C—S bond β-scission and the formations of CSC(=O)C ketone and Y(CSCO)C and CSY(CCO) ring structures are close to each other above 700 K and are all enhanced by higher temperature. Under a temperature below 400 K, the most and least important reactions besides the isomerization of and O_2 dissociation from $CH_3SCH(OO•)CH_3$ adduct are HO_2 elimination from $CH_3SCH(OO•)CH_3$ and Y(CSCO)C formation by $CH_2•SCH(OOH)CH_3$, respectively.

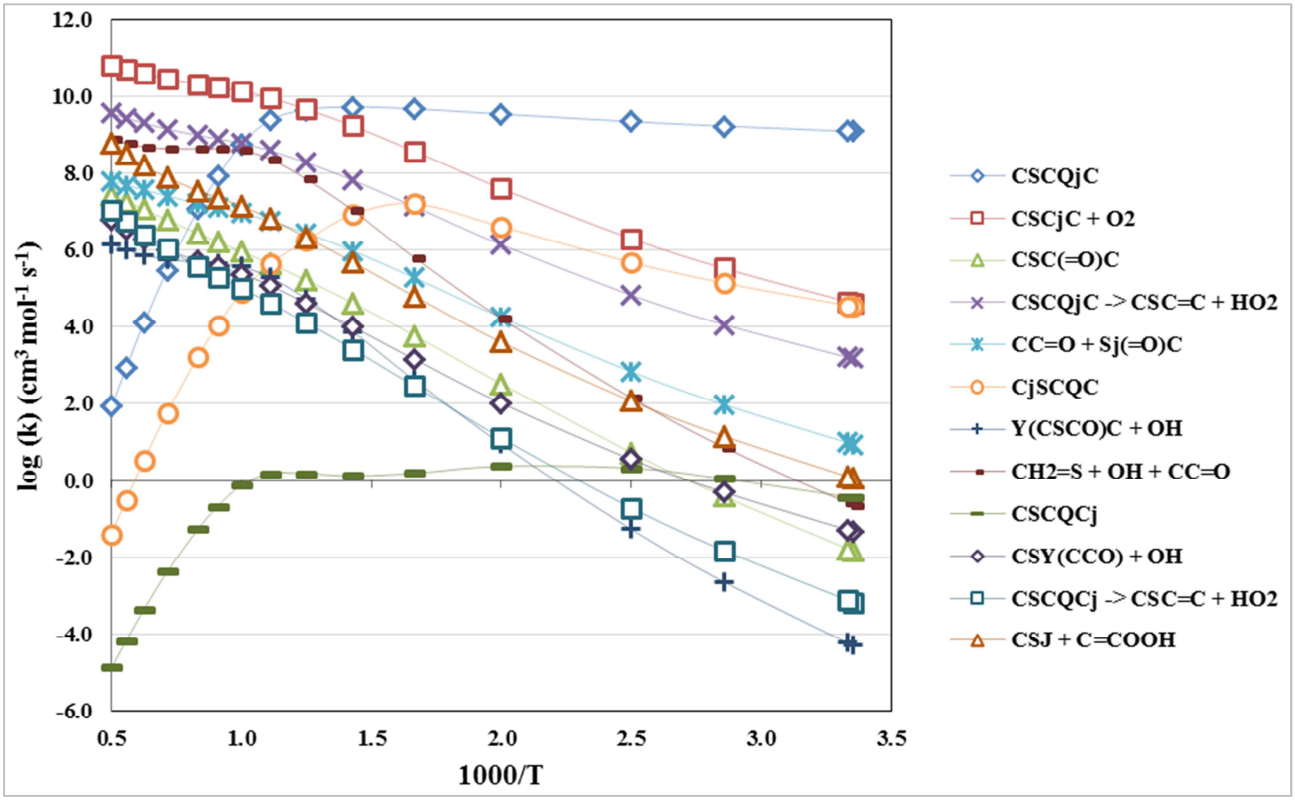

Figure 5. *Rate constant vs. temperature for the $CH_3SCH•CH_3$ + O_2 reaction system under P=1 atm, where "j" represents the location of radical site.*

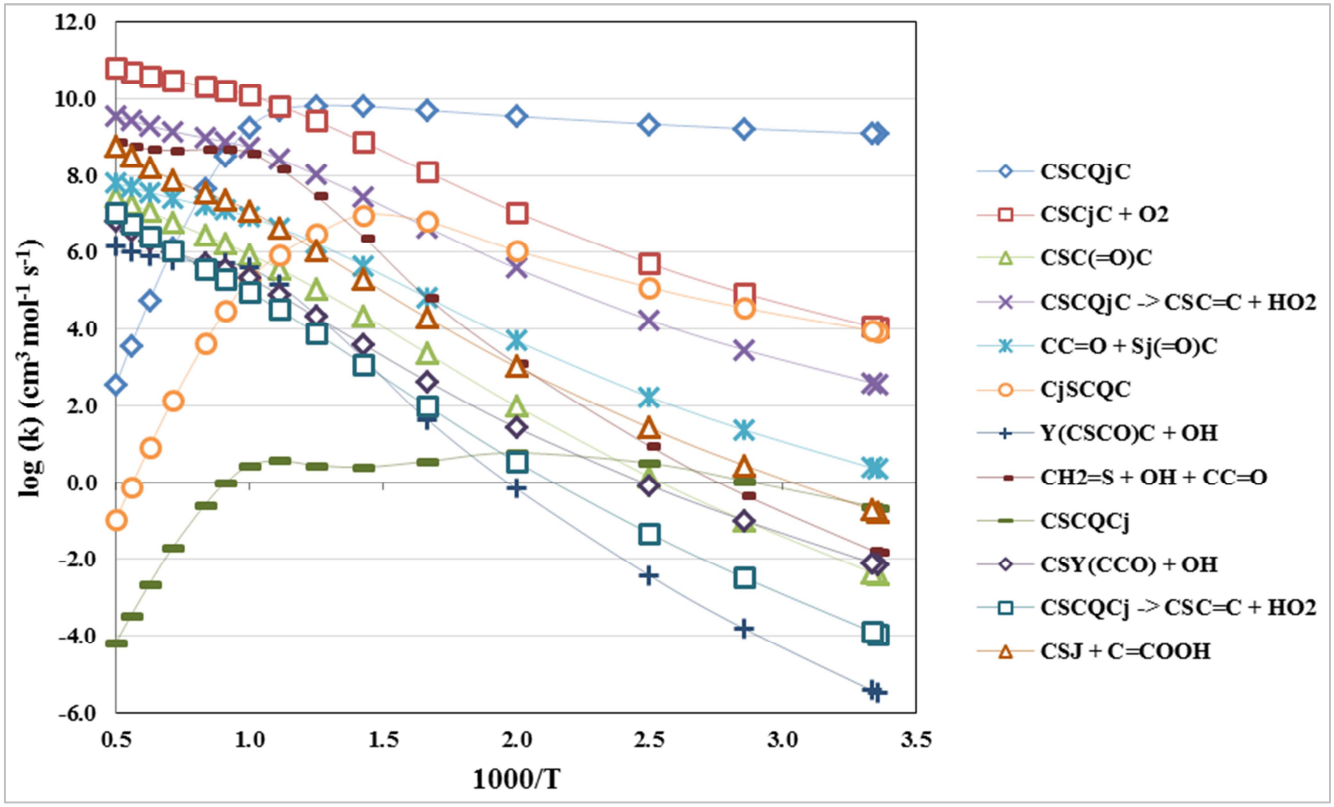

Figure 6. *Rate constant vs. temperature for the $CH_3SCH•CH_3 + O_2$ reaction system under P=4 atm, where "j" represents the location of radical site.*

The plots of reaction rate versus pressure under T=298 K and T=700 K are given by Figures 7 and 8, respectively. 700 K is chosen as a typical temperature of sulfuric compound combustion and pyrolysis. [2, 57-59]

Under T=298 K, the stabilization, dissociation and isomerization of $CH_3SCH(OO•)CH_3$ adduct are independent of pressure under room temperature. Reaction rates of C—S and O—O bond β-scission, HO_2 elimination, ring structure formation and CSC(=O)C ketone formation are enhanced under lower pressure. Stabilization to the peroxy radical, intramolecular hydrogen shift generating $CH_2•SCH(OOH)CH_3$, O_2 dissociation and HO_2 elimination from $CH_2•SCH(OOH)CH_3$ are the most important reactions under all pressures. The rates of intramolecular hydrogen shift leading to $CH_2SCH(OOH)CH_2•$ are about 4-5 orders of magnitude lower than those leading to $CH_2•SCH(OOH)CH_3$. HO_2 elimination from $CH_2SCH(OOH)CH_2•$ and y(CSCO)C formation are among the least important reactions and decrease under higher pressure.

Compared to T=298 K, Figure 8 indicates the pressure has stronger effects on reaction rates under T=700 K. Peroxy radical stabilization remains independent of pressure when temperature rises from 298 to 700 K. Under T=700 K intramolecular hydrogen shift leading to $CH_2SCH(OOH)CH_2•$ is the least important reaction and is significantly slower than that leading to $CH_2•SCH(OOH)CH_3$.

A higher pressure reduces all reactions besides the isomerization of and O_2 dissociation from the peroxy radical. Peroxy radical stabilization, O_2 dissociation and HO_2 elimination from peroxy radical, $CH_2•SCH(OOH)CH_3$ generation, and $CH_2•S$--$CH(OOH)CH_3$ bond β-scission leading to CH_2=S, OH and CC=O are the most important reactions under T=700 K within the pressure range of 0.5-20.0 atm. $CH_3SCH(OO•)CH_3$ dissociation via peroxy radical addition to the sulfur atom is significantly enhanced by increasing the temperature from 298 to 700 K. Meanwhile, decreasing the pressure from 1 to 0.5 atm does not alter any reaction rate under 298 or 700 K. Hence there is no need to pressurize or vacuumize the reaction system to make the $CSC•C + O_2$ reaction system move forward.

Hence Figures 5 and 6 indicate the temperature of 600-800K is recommended for the $CH_3SCH•CH_3 + O_2$ reaction system to move forward within the pressure range of 1-4 atm.

4. Summary

Thermochemical and kinetic studies of the $CH_3SCH•CH_3 + O_2$ reaction system are presented. The CBS-QB3 composite method of calculation is recommended for the oxidation of organosulfur compounds. The presence of sulfur reduces the chemical activation energy for $^3O_2$ association to secondary carbon atoms adjacent to the sulfur moiety by about 7 kcal/mol. The sulfur presents new paths in molecular dissociation by C—S bond β-scission and formations of aldehydes and sulfur – oxygen bond systems.

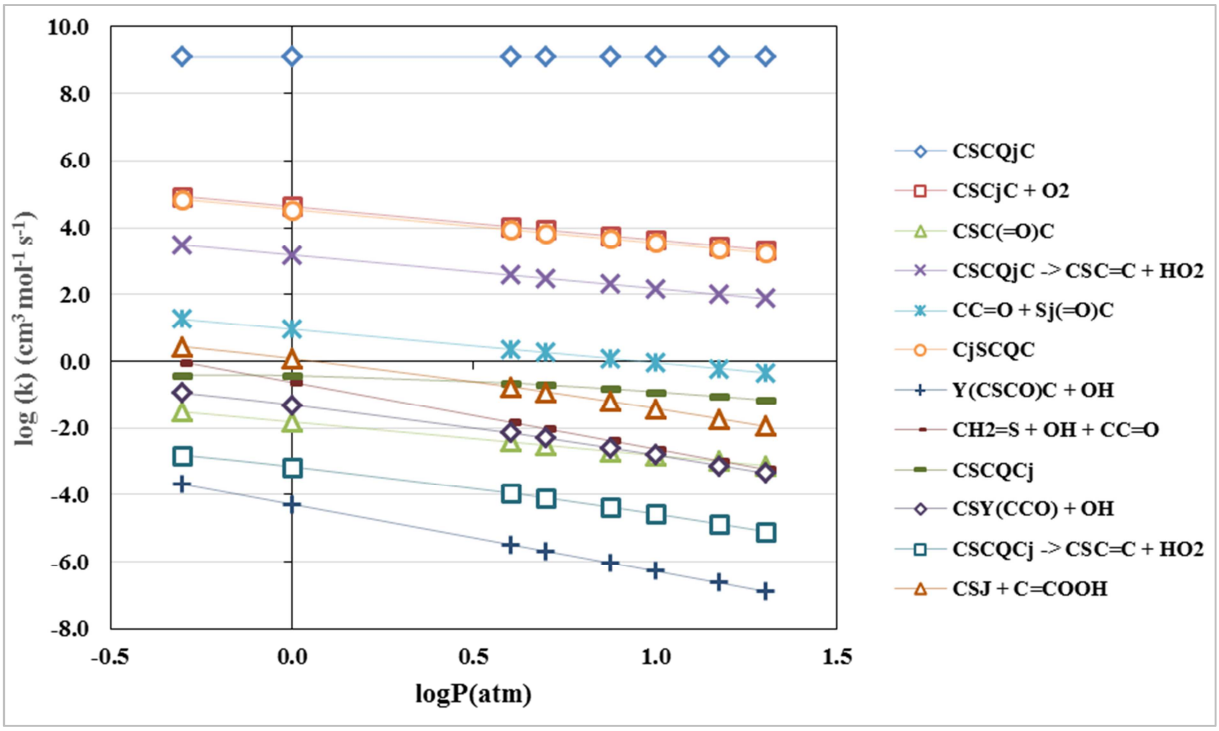

Figure 7. *Rate constant vs. pressure for the $CH_3SCH•CH_3 + O_2$ reaction system under T= 298 K, where "j" represents the location of radical site.*

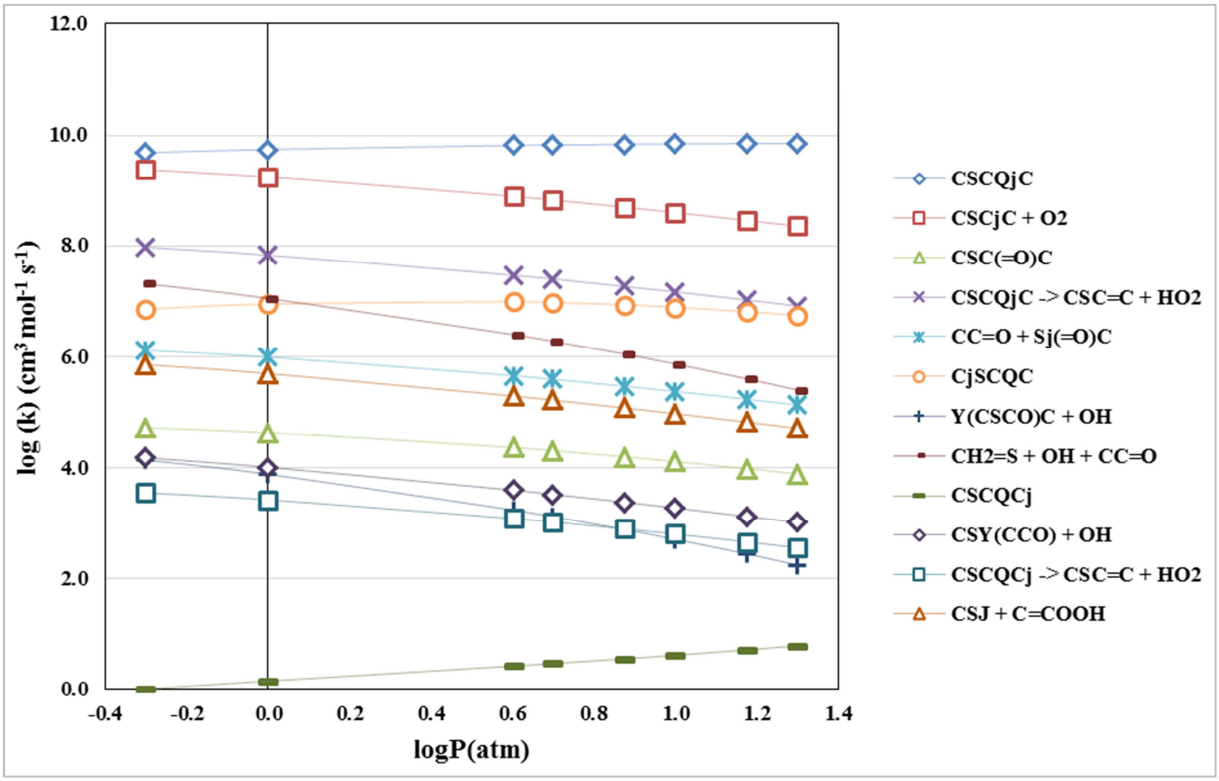

Figure 8. *Rate constant vs. pressure for the $CH_3SCH•CH_3 + O_2$ reaction system under T= 700 K, where "j" represents the location of radical site.*

Several new reaction paths are presented. These involve addition of the newly formed peroxy oxygen radical to the sulfur with cleavage of the sulfur – carbon bond, which allows the carbon – oxygen carbonyl bond to form.

$$C•SC(OOH)C \rightarrow CH_2=S + CC=O + OH \ (\Delta H_{rxn} = -7.0 \text{ kcal/mol})$$

$$CSC(OOH)C• \rightarrow CH_3S• + C=COOH \ (\Delta H_{rxn} = 8.5 \text{ kcal/mol})$$

$$CSC(OO•)C \rightarrow CC=O + CS•=O \ (\Delta H_{rxn} = -53.3 \text{ kcal/mol})$$

Rate constants vs. pressure at 300 and 700K and rate constants vs 1000/T(K) at 1 and 4 atm pressure are presented.

Rising the pressure from 0.5 to 20 atm does not significantly affect any elementary reaction step in the $CH_3SCH•CH_3 + O_2$ reaction system under either 298 or 700 K. Stabilization of $CH_3SCH(OO•)CH_3$ adduct is dominant below 500 K and minor above 900 K.

The two paths of $CH_3SCH(OO•)CH_3$ adduct isomerization by intramolecular hydrogen transfer are important in the temperature regime 400-800K. All the subsequent reactions of $CH_3SCH(OO•)CH_3$ adduct and its isomers are significantly enhanced by increasing the temperature from 298 to 700 K or higher.

The CBS-QB3, G3MP2B3 composite and M062x/6-311+G(2d,p) DFT methods are recommended for sulfuric compound oxidation reactions.

Supporting Information Description

Information about the inputs and outputs of Chemaster code, vibrational frequencies of the transition states under the CBS-QB3 level, and reduced set vibration frequencies under the CBS-QB3 level are given in the Supporting Information.

Acknowledgements

We acknowledge the NJIT Academic and Research Computing Systems resources and staff, for computational facilities and assistance on the "Kong HPC" computer system.

References

[1] K. Vijayaraghavan, K. Hemanathan, Biodiesel production from freshwater algae, Energy and Fuels 23 (2009) 5448-5453.

[2] F. G. Cerru, A. Kronenburg, R. P. Lindstedt, Systematically reduced chemical mechanisms for sulfur oxidation and pyrolysis, Combustion and Flame 146 (2006) 437-455.

[3] L. Hindiyarti, P. Glarborg, P. Marshall, Reactions of SO_3 with the O/H radical pool under combustion conditions, Journal of Physical Chemistry A 111 (2007) 3984-3991.

[4] I. A. Gargurevich, Hydrogen sulfide combustion: Relevant issues under claus furnace conditions, Industrial and Engineering Chemistry Research 44 (2005) 7706-7729.

[5] A. Gross, I. Barnes, R. M. Sørensen, J. Kongsted, K. V. Mikkelsen, A Theoretical Study of the Reaction between $CH_3S(OH)CH_3$ and O_2, The Journal of Physical Chemistry A 108 (2004) 8659-8671.

[6] M. B. Williams, P. Campuzano-Jost, A. J. Pounds, A. J. Hynes, Experimental and theoretical studies of the reaction of the OH radical with alkyl sulfides: 2. Kinetics and mechanism of the OH initiated oxidation of methylethyl and diethyl sulfides; observations of a two channel oxidation mechanism, Physical Chemistry Chemical Physics 9 (2007) 4370-4382.

[7] M. B. Williams, P. Campuzano-Jost, A. J. Hynes, A. J. Pounds, Experimental and theoretical studies of the reaction of the OH radical with alkyl sulfides: 3. Kinetics and mechanism of the OH initiated oxidation of dimethyl, dipropyl, and dibutyl sulfides: reactivity trends in the alkyl sulfides and development of a predictive expression for the reaction of OH with DMS, Journal of Physical Chemistry A 113 (2009) 6697-6709.

[8] J. Cao, W. Wang, Y. Zhang, T. Zhang, J. Lv, C. Li, Computational study on the reaction of $CH_3SCH_2CH_3$ with OH radical: Mechanism and enthalpy of formation, Theoretical Chemistry Accounts 129 (2011) 771-780.

[9] S. Pillai, J. W. Bozzelli, Computational study on structures, thermochemical properties, and bond energies of disulfide oxygen (S-S-O)-bridged CH 3SSOH and CH 3SS(=O)H and radicals, Journal of Physical Organic Chemistry 25 (2012) 475-485.

[10] C. S. Turchi, D. F. Ollis, Photocatalytic degradation of organic water contaminants: Mechanisms involving hydroxyl radical attack, Journal of Catalysis 122 (1990) 178-192.

[11] D. Grosjean, Photooxidation of methyl sulfide, ethyl sulfide, and methanethiol, Environmental Science and Technology 18 (1984) 460-468.

[12] A. J. Hynes, P. H. Wine, D. H. Semmes, Kinetics and mechanism of OH reactions with organic sulfides, Journal of Physical Chemistry 90 (1986) 4148-4156.

[13] M. B. Williams, P. Campuzano-Jost, B. M. Cossairt, A. J. Hynes, A. J. Pounds, Experimental and theoretical studies of the reaction of the OH radical with alkyl sulfides: 1. Direct observations of the formation of the OH-DMS adduct-pressure dependence of the forward rate of addition and development of a predictive expression at low temperature, Journal of Physical Chemistry A 111 (2007) 89-104.

[14] S. P. Pillai, Structure and Thermochemistry of Disulfide-Oxygen Species, Department of Chemistry and Environmental Science, New Jersey Institute of Technology, Newark, NJ, 2008.

[15] A. G. Vandeputte, M. -F. Reyniers, G. B. Marin, Theoretical Study of the Thermal Decomposition of Dimethyl Disulfide, Journal of Physical Chemistry A 114 (2010) 10531-10549.

[16] X. Zheng, J. W. Bozzelli, E. M. Fisher, F. C. Gouldin, L. Zhu, Experimental and computational study of oxidation of diethyl sulfide in a flow reactor, Proceedings of the Combustion Institute 33 (2011) 467-475.

[17] G. Oksdath-Mansilla, A. B. Peñéñory, I. Barnes, P. Wiesen, M. A. Teruel, Photodegradation of (CH 3CH 2) 2S and CH 3CH 2SCH 3 initiated by OH radicals at atmospheric pressure. Product yields and mechanism in NOx free air, Atmospheric Environment 55 (2012) 263-270.

[18] J. A. Pople, M. Head-Gordon, D. J. Fox, K. Raghavachari, L. A. Curtiss, Gaussian-1 theory: A general procedure for prediction of molecular energies, The Journal of Chemical Physics 90 (1989) 5622-5629.

[19] J. A. Pople, Nobel lecture: Quantum chemical models, Reviews of Modern Physics 71 (1999) 1267-1274.

[20] M. J. Frisch, G. W. Trucks, H. B. Schlegel, G. E. Scuseria, M. A. Robb, J. R. Cheeseman, J. A. Montgomery, T. Vreven, K. N. Kudin, J. C. Burant, J. M. Millam, S. S. Iyengar, J. Tomasi, V. Barone, B. Mennucci, M. Cossi, G. Scalmani, N. Rega, G. A. Petersson, H. Nakatsuji, M. Hada, M. Ehara, K. Toyota, R. Fukuda, J. Hasegawa, M. Ishida, T. Nakajima, Y. Honda, O. Kitao, H. Nakai, M. Klene, X. Li, J. E. Knox, H. P. Hratchian, J. B. Cross, V. Bakken, C. Adamo, J. Jaramillo, R. Gomperts, R. E. Stratmann, O. Yazyev, A. J. Austin, R. Cammi, C. Pomelli, J. W. Ochterski, P. Y. Ayala, K. Morokuma, G. A. Voth, P. Salvador, J. J. Dannenberg, V. G. Zakrzewski, S. Dapprich, A. D. Daniels, M. C. Strain, O. Farkas, D. K. Malick, A. D. Rabuck, K. Raghavachari, J. B. Foresman, J. V. Ortiz, Q. Cui, A. G. Baboul, S. Clifford, J. Cioslowski, B. B. Stefanov, G. Liu, A. Liashenko, P. Piskorz, I. Komaromi, R. L. Martin, D. J. Fox, T. Keith, A. Laham, C. Y. Peng, A. Nanayakkara, M. Challacombe, P. M. W. Gill, B. Johnson, W. Chen, M. W. Wong, C. Gonzalez, J. A. Pople, Gaussian 03, Revision C. 02, 2003.

[21] J. A. Montgomery Jr, M. J. Frisch, J. W. Ochterski, G. A. Petersson, A complete basis set model chemistry. VII. Use of the minimum population localization method, Journal of Chemical Physics 112 (2000) 6532-6542.

[22] J. A. Montgomery Jr, M. J. Frisch, J. W. Ochterski, G. A. Petersson, A complete basis set model chemistry. VI. Use of density functional geometries and frequencies, Journal of Chemical Physics 110 (1999) 2822-2827.

[23] L. A. Curtiss, P. C. Redfern, K. Raghavachari, V. Rassolov, J. A. Pople, Gaussian-3 theory using reduced Møller-Plesset order, Journal of Chemical Physics 110 (1999) 4703-4709.

[24] A. G. Baboul, L. A. Curtiss, P. C. Redfern, K. Raghavachari, Gaussian-3 theory using density functional geometries and zero-point energies, Journal of Chemical Physics 110 (1999) 7650-7657.

[25] L. A. Curtiss, K. Raghavach Ari, P. C. Redfern, V. Rassolov, J. A. Pople, Gaussian-3 (G3) theory for molecules containing first and second-row atoms, Journal of Chemical Physics 109 (1998) 7764-7776.

[26] K. B. Wiberg, G. A. Petersson, A Computational Study of RXHn X-H Bond Dissociation Enthalpies, Journal of Physical Chemistry A 118 (2014) 2353-2359.

[27] K. B. Wiberg, G. B. Ellison, J. M. McBride, G. A. Petersson, Substituent Effects on O-H Bond Dissociation Enthalpies: A Computational Study, Journal of Physical Chemistry A 117 (2013) 213-218.

[28] V. G. Kiselev, N. P. Gritsan, V. E. Zarko, P. I. Kalmykov, V. A. Shandakov, Multilevel quantum chemical calculation of the enthalpy of formation of 1,2,5 oxadiazolo 3,4-e 1,2,3,4 - tetrazine-4,6-Di-N-Dioxide, Combustion Explosion and Shock Waves 43 (2007) 562-566.

[29] C. Y. Sheng, J. W. Bozzelli, A. M. Dean, A. Y. Chang, Detailed Kinetics and Thermochemistry of $C_2H_5 + O_2$: Reaction Kinetics of the Chemically-Activated and Stabilized $CH_3CH_2OO•$ Adduct, The Journal of Physical Chemistry A 106 (2002) 7276-7293.

[30] K. B. Wiberg, Ab Initio Molecular Orbital Theory, J. Comput. Chem. 7 (1986) 379-379.

[31] I. K. Ortega, O. Kupiainen, T. Kurtén, T. Olenius, O. Wilkman, M. J. McGrath, V. Loukonen, H. Vehkamäki, From quantum chemical formation free energies to evaporation rates, Atmospheric Chemistry and Physics 12 (2012) 225-235.

[32] R. Casasnovas, J. Frau, J. Ortega-Castro, A. Salvà, J. Donoso, F. Muñoz, Simplification of the CBS-QB3 method for predicting gas-phase deprotonation free energies, International Journal of Quantum Chemistry 110 (2010) 323-330.

[33] A. G. Vandeputte, M. K. Sabbe, M. F. Reyniers, G. B. Marin, Modeling the Gas-Phase Thermochemistry of Organosulfur Compounds, Chemistry-a European Journal 17 (2011) 7656-7673.

[34] C. A. Class, J. Aguilera-Iparraguirre, W. H. Green, A kinetic and thermochemical database for organic sulfur and oxygen compounds, Physical Chemistry Chemical Physics 17 (2015) 13625-13639.

[35] A. D. Becke, Density-functional thermochemistry. III. The role of exact exchange, The Journal of Chemical Physics 98 (1993) 5648-5652.

[36] T. H. Lay, L. N. Krasnoperov, C. A. Venanzi, J. W. Bozzelli, N. V. Shokhirev, Ab initio study of α-chlorinated ethyl hydroperoxides CH_3CH_2OOH, $CH_3CHClOOH$, and CH_3CCl_2OOH: Conformational analysis, internal rotation barriers, vibrational frequencies, and thermodynamic properties, Journal of Physical Chemistry 100 (1996) 8240-8249.

[37] H. Wang, Á. Castillo, J. W. Bozzelli, Thermochemical Properties Enthalpy, Entropy, and Heat Capacity of C1–C4 Fluorinated Hydrocarbons: Fluorocarbon Group Additivity, The Journal of Physical Chemistry A 119 (2015) 8202-8215.

[38] B. A. Ellingson, V. A. Lynch, S. L. Mielke, D. G. Truhlar, Statistical thermodynamics of bond torsional modes: Tests of separable, almost-separable, and improved Pitzer-Gwinn approximations, Journal of Chemical Physics 125 (2006).

[39] P. Hui-Yun, The modified Pitzer-Gwinn method for partition function of restricted internal rotation of a molecule, The Journal of Chemical Physics 87 (1987) 4846-4848.

[40] K. S. Pitzer, Thermodynamic functions for molecules having restricted internal rotations, The Journal of Chemical Physics 5 (1937) 469-472.

[41] G. da Silva, J. W. Bozzelli, Enthalpies of formation, bond dissociation energies, and molecular structures of the n-aldehydes (acetaldehyde, propanal, butanal, pentanal, hexanal, and heptanal) and their radicals, Journal of Physical Chemistry A 110 (2006) 13058-13067.

[42] S. R. Hashemi, V. Saheb, Theoretical studies on the mechanism and kinetics of the hydrogen abstraction reactions of threo-CF3CHFCHFC2F5 and erythro-CF3CHFCHFC2F5 (HFC-43-10mee) by OH radicals, Computational and Theoretical Chemistry 1119 (2017) 59-64.

[43] H. S. Johnston, J. Heicklen, TUNNELLING CORRECTIONS FOR UNSYMMETRICAL ECKART POTENTIAL ENERGY BARRIERS, The Journal of Physical Chemistry 66 (1962) 532-533.

[44] H. S. Johnston, Gas phase reaction rate theory, New York, Ronald Press Co. [1966] 1966.

[45] S. Yommee, J. W. Bozzelli, Cyclopentadienone Oxidation Reaction Kinetics and Thermochemistry for the Alcohols, Hydroperoxides, and Vinylic, Alkoxy, and Alkylperoxy Radicals, Journal of Physical Chemistry A 120 (2016) 433-451.

[46] F. Jin, R. Asatryan, J. W. Bozzelli, Thermodynamic and kinetic analysis on the reaction of dimethyl sulfide radical with oxygen, International Journal of Quantum Chemistry 112 (2012) 1945-1958.

[47] S. Snitsiriwat, J. W. Bozzelli, Thermochemistry, reaction paths, and kinetics on the tert -isooctane radical reaction with O_2, Journal of Physical Chemistry A 118 (2014) 4631-4646.

[48] H. Wang, J. W. Bozzelli, Thermochemistry and Kinetic Analysis of the Unimolecular Oxiranyl Radical Dissociation Reaction: A Theoretical Study, Chem Phys Chem, doi: 10.1002/cphc.201600152(2016).

[49] B. E. Poling, J. M. Prausnitz, J. P. O'Connell, The properties of gases and liquids, New York: McGraw-Hill, c2001. 5th ed. 2001.

[50] R. Atkinson, J. Arey, Atmospheric Degradation of Volatile Organic Compounds, Chemical Reviews 103 (2003) 4605-4638.

[51] G. Oksdath-Mansilla, A. B. Peñéñory, M. Albu, I. Barnes, P. Wiesen, M. A. Teruel, FTIR relative kinetic study of the reactions of $CH_3CH_2SCH_2CH_3$ and $CH_3CH_2SCH_3$ with OH radicals and Cl atoms at atmospheric pressure, Chemical Physics Letters 477 (2009) 22-27.

[52] L. Zhu, J. W. Bozzelli, L. M. Kardos, Thermochemical properties, Δ fH o (298), S o (298), and C p o (298), (T), for n-butyl and n-pentyl hydroperoxides and the alkyl and peroxy radicals, transition states, and kinetics for intramolecular hydrogen shift reactions of the peroxy radicals, Journal of Physical Chemistry A 111 (2007) 6361-6377.

[53] G. Song, J. W. Bozzelli, Structures and thermochemistry of methyl ethyl sulfide and its hydroperoxides: $HOOCH_2SCH_2CH3$, $CH_3SCH(OOH)CH_3$, $CH_3SCH_2CH_2OOH$, and radicals, Journal of Physical Organic Chemistry, doi: 10.1002/poc.3751 e3751-n/a.

[54] G. Song, J. W. Bozzelli, Structural and thermochemical studies on CH_3SCH_2CHO, CH_3CH_2SCHO, $CH_3SC(=O)CH3$, and radicals corresponding to loss of H atom, Journal of Physical Organic Chemistry, doi: 10.1002/poc.3688(2017) e3688-n/a.

[55] B. Ruscic, Active Thermochemical Tables: Sequential Bond Dissociation Enthalpies of Methane, Ethane, and Methanol and the Related Thermochemistry, Journal of Physical Chemistry A 119 (2015) 7810-7837.

[56] C. F. Goldsmith, G. R. Magoon, W. H. Green, Database of small molecule thermochemistry for combustion, Journal of Physical Chemistry A 116 (2012) 9033-9047.

[57] Z. Xin, E. M. Fisher, F. C. Gouldin, J. W. Bozzelli, Pyrolysis and oxidation of ethyl methyl sulfide in a flow reactor, Combustion and Flame 158 (2011) 1049-1058.

[58] X. Zheng, E. M. Fisher, F. C. Gouldin, L. Zhu, J. W. Bozzelli, Experimental and computational study of diethyl sulfide pyrolysis and mechanism, Proceedings of the Combustion Institute 32 (2009) 469-476.

[59] K. P. Somers, J. M. Simmie, F. Gillespie, C. Conroy, G. Black, W. K. Metcalfe, F. Battin-Leclerc, P. Dirrenberger, O. Herbinet, P. -A. Glaude, P. Dagaut, C. Togbé, K. Yasunaga, R. Fernandes, C. Lee, R. Tripathi, H. J. Curran, A comprehensive experimental and detailed chemical kinetic modelling study of 2,5-dimethylfuran pyrolysis and oxidation, Combustion and Flame 160 (2013) 2291-2318.